Search for Solar Axions by the CERN Axion Solar Telescope with ^{3}He Buffer Gas: Closing the Hot Dark Matter Gap

M. Arik,[1,a] S. Aune,[2] K. Barth,[3] A. Belov,[4] S. Borghi,[3,b] H. Bräuninger,[5] G. Cantatore,[6] J. M. Carmona,[7] S. A. Cetin,[1] J. I. Collar,[8] E. Da Riva,[3] T. Dafni,[7,c] M. Davenport,[3] C. Eleftheriadis,[9] N. Elias,[3,d] G. Fanourakis,[10] E. Ferrer-Ribas,[2] P. Friedrich,[5] J. Galán,[7,2] J. A. García,[7] A. Gardikiotis,[11] J. G. Garza,[7] E. N. Gazis,[12] T. Geralis,[10] E. Georgiopoulou,[11] I. Giomataris,[2] S. Gninenko,[4] H. Gómez,[7,e] M. Gómez Marzoa,[3,f] E. Gruber,[13] T. Guthörl,[13] R. Hartmann,[14,g] S. Hauf,[15,h] F. Haug,[3] M. D. Hasinoff,[16] D. H. H. Hoffmann,[15] F. J. Iguaz,[7,2] I. G. Irastorza,[7] J. Jacoby,[17] K. Jakovčić,[18] M. Karuza,[6,i] K. Königsmann,[13] R. Kotthaus,[19] M. Krčmar,[18] M. Kuster,[5,15,h] B. Lakić,[18] P. M. Lang,[15] J. M. Laurent,[3] A. Liolios,[9] A. Ljubičić,[18] G. Luzón,[7] S. Neff,[15] T. Niinikoski,[3,j] A. Nordt,[5,15,d] T. Papaevangelou,[2] M. J. Pivovaroff,[20] G. Raffelt,[19] H. Riege,[15] A. Rodríguez,[7] M. Rosu,[15] J. Ruz,[3,20] I. Savvidis,[9] I. Shilon,[7,3,k] P. S. Silva,[3] S. K. Solanki,[21,l] L. Stewart,[3] A. Tomás,[7] M. Tsagri,[11,3] K. van Bibber,[20,m] T. Vafeiadis,[3,9,11] J. Villar,[7] J. K. Vogel,[13,20] S. C. Yildiz,[1,a] K. Zioutas[3,11]

(CAST Collaboration)

[1]*Dogus University, Istanbul, Turkey*
[2]*IRFU, Centre d'Études Nucléaires de Saclay (CEA-Saclay), Gif-sur-Yvette, France*
[3]*European Organization for Nuclear Research (CERN), Genève, Switzerland*
[4]*Institute for Nuclear Research (INR), Russian Academy of Sciences, Moscow, Russia*
[5]*Max-Planck-Institut für Extraterrestrische Physik, Garching, Germany*
[6]*Istituto Nazionale di Fisica Nucleare (INFN), Sezione di Trieste and Università di Trieste, Trieste, Italy*
[7]*Grupo de Investigación de Física Nuclear y Astropartículas, Universidad de Zaragoza, Zaragoza, Spain*
[8]*Enrico Fermi Institute and KICP, University of Chicago, Chicago, Illinois 60637, Illinois, USA*
[9]*Aristotle University of Thessaloniki, Thessaloniki, Greece*
[10]*National Center for Scientific Research "Demokritos", Athens, Greece*
[11]*Physics Department, University of Patras, Patras, Greece*
[12]*National Technical University of Athens, Athens, Greece*
[13]*Albert-Ludwigs-Universität Freiburg, Freiburg, Germany*
[14]*MPI Halbleiterlabor, München, Germany*
[15]*Technische Universität Darmstadt, IKP, Darmstadt, Germany*
[16]*Department of Physics and Astronomy, University of British Columbia, Vancouver, Canada*
[17]*Johann Wolfgang Goethe-Universität, Institut für Angewandte Physik, Frankfurt am Main, Germany*
[18]*Rudjer Bošković Institute, Zagreb, Croatia*
[19]*Max-Planck-Institut für Physik (Werner-Heisenberg-Institut), München, Germany*
[20]*Lawrence Livermore National Laboratory, Livermore, California 94550, California, USA*
[21]*Max-Planck-Institut für Sonnensystemforschung, Göttingen, Germany*

(Received 9 July 2013; revised manuscript received 26 December 2013; published 4 March 2014)

The CERN Axion Solar Telescope has finished its search for solar axions with ^{3}He buffer gas, covering the search range $0.64\ \text{eV} \lesssim m_a \lesssim 1.17\ \text{eV}$. This closes the gap to the cosmological hot dark matter limit and actually overlaps with it. From the absence of excess x rays when the magnet was pointing to the Sun we set a typical upper limit on the axion-photon coupling of $g_{a\gamma} \lesssim 3.3 \times 10^{-10}\ \text{GeV}^{-1}$ at 95% C.L., with the exact value depending on the pressure setting. Future direct solar axion searches will focus on increasing the sensitivity to smaller values of $g_{a\gamma}$, for example by the currently discussed next generation helioscope International AXion Observatory.

DOI: 10.1103/PhysRevLett.112.091302 PACS numbers: 95.35.+d, 14.80.Va, 96.60.Vg

Introduction.—The most promising method to search for axions and axion-like particles (ALPs) [1–4], low-mass bosons with a two-photon interaction vertex, is their conversion to photons in macroscopic magnetic fields [5–7]. This approach includes the search for solar axions by the helioscope technique [8–15], photon regeneration experiments ("shining light through a wall") [16–18], axion-photon conversion in astrophysical B fields [19–22], and the search for galactic axion dark matter [23–27].

One limiting factor in any of these efforts is the momentum difference between freely propagating photons and axions caused by the axion mass m_a. It limits the magnetic field volume over which the conversion is coherent. In solar axion searches one can extend the search to larger m_a values by providing the photons with a refractive mass [28]. The conversion pipe is filled with a low-Z buffer gas; the search mass is chosen by adjusting the gas pressure. In this way, the CERN Axion Solar Telescope (CAST), the largest axion helioscope to date, has successively pushed its search range to higher m_a values (see Fig. 1 for a summary of results). We here report on the final search range based on ^{3}He buffer gas.

Within the ALP family of hypothetical bosons, the original axion is the best-motivated case because it emerges from the compelling Peccei-Quinn mechanism to explain the absence of CP-violating effects in QCD. In the two-dimensional $g_{a\gamma}$-m_a ALP parameter space, the QCD axion must lie somewhere on a line $g_{a\gamma} \propto m_a$. The close relationship between axions and neutral pions implies that this line is anchored to the point describing the π^0 mass and the pion-photon coupling constant. After allowing for model-dependent numerical factors, the axion may be found anywhere in the yellow band indicated in Fig. 1. The CAST vacuum result ($g_{a\gamma} < 0.88 \times 10^{-10}$ GeV^{-1} at 95% C.L. for $m_a \lesssim 0.02$ eV [13]) remains a milestone in the ALP landscape. However, a major objective of CAST has been to find or exclude QCD axions and thus to push as far as possible to higher m_a values. Our first ^{3}He limits [15] have for the first time crossed the axion line appropriate for the Kim-Shifman-Vainshtein-Zakharov (KSVZ) model (Fig. 1) [32,33].

QCD axions with parameters in this range thermalize in the early Universe after the QCD phase transition by interactions with pions [34] and would thus exist with a present-day number density of around 50 cm^{-3}, comparable to 0.5 neutrino species, and are therefore susceptible to hot dark matter bounds [31,35,36]. Assuming neutrino masses to be negligible, the latest axion hot dark matter bound is $m_a \lesssim 0.9$ eV, leaving a small gap to our earlier ^{3}He search range, which we now close.

The recent Planck measurements of the cosmic microwave background significantly improve our knowledge of many cosmological parameters. In contrast to earlier cosmic microwave background results, Planck alone now constrains the axion mass and provides a limit $m_a <$ 1.01 eV (95% C.L.) [37]. The inclusion of other data sets, notably the matter power spectrum and the HST measurement of the Hubble parameter, have only a small impact, providing limits between 0.67 and 0.86 eV, depending on the combination of data sets [37]. In other words, concerning a possible axion hot dark matter contribution to the universe, the situation after Planck is almost the same as before.

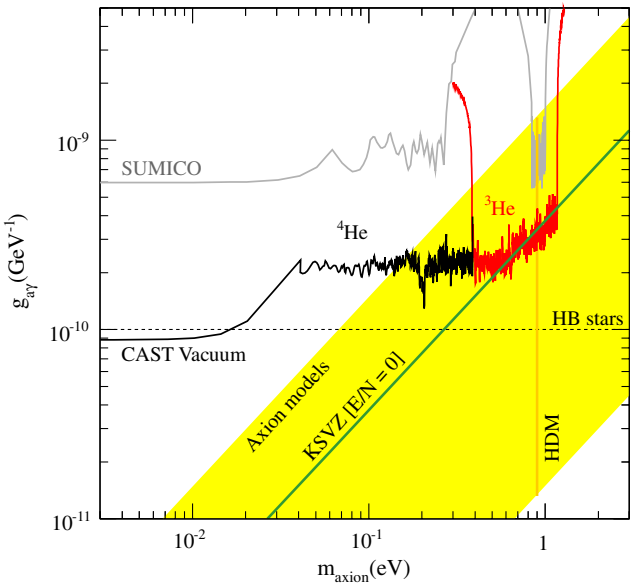

FIG. 1 (color online). Exclusion regions in the m_a-$g_{a\gamma}$ plane achieved by CAST in vacuum [12,13], ^{4}He [14], and the first part of the ^{3}He phase, [15], and our new results (all in red). We also show constraints from Sumico [9–11], horizontal branch (HB) stars [29] (a somewhat more restrictive limit stems from blue-loop suppression in massive stars [30]), and the hot dark matter (HDM) bound [31]. The yellow band represents typical theoretical models with $|E/N - 1.95| = 0.07$–7. The green solid line corresponds to $E/N = 0$ (KSVZ model).

System description and data-taking strategy.—CAST uses a straight 10 m LHC test dipole magnet ($B \sim 9.0$ T), mounted on a movable platform to follow the Sun for about 1.5 h both at sunrise and sunset. The two bores extend beyond the cold mass (length 10.25 m) for 16 cm on each side forming four link regions, which are closed by x-ray cold windows. The volume of the two cold bores is 30 L and the total volume of the link regions is 1.5 L. The magnetic field length of 9.26 m is centrally located within the cold mass. One of the apertures of the magnet is covered by a CCD/Telescope system [38] and the others by three Micromegas detectors of the microbulk type [39–42]. The axion-photon conversion probability when the conversion volume is filled with a buffer gas (^{3}He in our case) is [14]

$$P_{a\to\gamma} = \left(\frac{Bg_{a\gamma}}{2}\right)^2 \frac{1 + e^{-\Gamma L} - 2e^{-\Gamma L/2}\cos(qL)}{q^2 + \Gamma^2/4}, \quad (1)$$

where the axion-photon momentum transfer provided by the magnetic field is $q = |m_a^2 - m_\gamma^2|/2E$ and Γ is the inverse photon absorption length in the buffer gas. The value of Γ varies with the pressure and the energy; for example, for a relatively high pressure of 70 mbar of ^{3}He, for the mean energy of the expected flux of 4.3 keV, $\Gamma = 0.156\ \mathrm{m}^{-1}$. The maximum conversion probability is reached for $m_a \simeq m_\gamma$ where m_γ is the photon refraction mass, which depends on the buffer gas density. For $m_a \neq m_\gamma$, the probability rapidly decreases due to the axion-photon momentum mismatch.

Throughout CAST Phase II, the data taking strategy was to increase the density in the cold bore circuit in small steps chosen to partially overlap the intrinsic mass acceptance ($\sim$1 meV FWHM) of the previous setting and so scan smoothly over the whole available mass range. The original step size and exposure time have been modified on a number of occasions in order to complete the physics program more efficiently without compromising continuity, but at the expense of reduced sensitivity at higher masses.

The central gas density inside the cold bore, with the magnet horizontal, is calculated from the cold bore pressure (P_{cb}) measured at one end, the magnet temperature T_{mag}, and the equation of state (EOS) of ^{3}He gas [43]. During solar tracking, P_{cb} changes continuously, as expected, due to the changing hydrostatic pressure of the ^{3}He gas column and due to a tilt-induced, slow characteristic temperature transient in the magnet (10–15 mK) from the cryogenic circuit. For example, at $P_{\mathrm{cb}} = 84$ mbar, a vertical movement of the magnet of 6 deg causes a shift in P_{cb} of $+1.06$ mbar. Hydrostatic and magnet temperature effects account for $+0.65$ mbar. The remaining contribution of 0.4 mbar we ascribe to changing fluid dynamics in the buffer gas at the extremities of the cold bore.

The fluid dynamics effect is driven by the presence of short relatively warm link regions; the ^{3}He temperature and density are not uniform throughout the whole system as regions with lighter vapor are present at the extremities, where buoyancy-driven flows occur. The magnet tilting affects such phenomena, giving rise to a redistribution of the ^{3}He mass and a consequent pressure change. To take the pressure and temperature variation into account, our analysis procedure continuously calculates the density during solar tracking. First, the pressure in the center of the magnet is calculated from the P_{cb} and the hydrostatic pressure difference. Then the density in the center is calculated from this central pressure and the temperature measurement (via the ^{3}He EOS). In this way the fluid dynamics effects on the measured pressure directly change the central density value.

Although the P_{cb} measurement allows us to calculate the central density at any moment, the actual density profile (which is needed to calculate the coherence length) and its variation on tilting cannot be measured directly and must be determined by computational fluid dynamics (CFD) simulations. The CFD simulations take into account all requisite physical phenomena, such as gravity, natural convection, and turbulence together with the geometry of the cold bores, link volumes, and the cold windows and the buffer gas EOS. The boundary conditions are defined by P_{cb}, T_{mag}, and several temperatures measured around the link volumes and cold window flanges.

An extensive and on-going program of CFD simulations has been undertaken and CAST has made detailed studies with a number of different models to find the best description of the measured behavior. The tilted and horizontal cases were treated separately. Various turbulence models were used for the horizontal case and a model forcing laminar flow was favored, while a composite model was devised for the tilted case as the most intuitive natural description of the system. This model consists of a turbulent solution in the lower half of the cold bore smoothly joined to a laminar solution in the upper half. The predicted pressure variations between tilted simulations at different vertical angles are in satisfactory agreement with those observed experimentally (e.g., within 0.06 mbar for 84 mbar).

For the analysis presented in this Letter, the density profiles derived from turbulent CFD simulations made with the magnet horizontal and over the full range of Phase II density settings were subjected to a simple and conservative coherence criterion ($\Delta\rho < 0.001\ \mathrm{kg\,m}^{-3}$). The resulting dependence of the effective coherence length L_{eff} with density was parametrized and applied to all data independent of photon energy and tilt angle. L_{eff} decreases from about 9 to 6 m in the range $m_a = 0.4$ eV to $m_a = 1.15$ eV, compared with the magnetic length of 9.26 m. To estimate the systematic error of such an approach, an analysis was done using a coherence length $L_{\mathrm{eff}} = 5.0$ m for all angles and masses. This extreme case is only found in laminar horizontal simulations at the highest pressures. The final effect on the limit on the $g_{a\gamma}$ from applying this simple criterion is well below 10%.

Data analysis and results.—The results presented in the Letter correspond to 1100 hour $\times$ detector taken by the three Micromegas detectors from 2009 to 2011 with ^{3}He in the system in axion-sensitive conditions (i.e., with the magnet tracking the Sun). Background levels are determined from a larger body of data taken during nontracking time. The data acquired by the CCD/Telescope of this period are under analysis and will be presented in a later publication. The present data correspond to about 418 effective axion mass steps that, together with the first 252 ^{3}He steps already released in a previous paper [15], continuously cover an axion mass range between 0.39 and 1.17 eV. Due to the density excursions experienced during a single tracking, data from each actual density step contribute to the neighbouring mass steps, especially for the larger densities used. The effective average exposure time per mass step is approximately 0.75 h per detector for

masses from 0.64 to 1 eV, while it was reduced to ~0.4 h detector for masses above 1 eV.

The data analysis is performed in a manner similar to our previous results [12–15]. We use an unbinned likelihood function that can be expressed as

$$\log \mathcal{L} \propto -R_T + \sum_i^N \log R(t_i, E_i, d_i). \quad (2)$$

Here R_T is the integrated expected number of counts over all exposure time, energy, and detectors. The sum runs over each of the N detected counts for the event rate $R(t_i, E_i, d_i)$ expected at the time t_i, energy E_i and detector d_i of the event i

$$R(t, E, d) = B_d + S(t, E, d), \quad (3)$$

where B_d is the background rate of detector d. $S(t, E, d)$ is the expected rate from axions in detector d, which depends on the axion properties $g_{a\gamma}$ and m_a

$$S(t, E, d) = \frac{d\Phi_a}{dE} P_{a\to\gamma} \epsilon_d, \quad (4)$$

where $P_{a\to\gamma}$ is the axion photon conversion probability in the CAST magnet given by Eq. (1) and ϵ_d is the detector effective area. Finally, the solar axion spectrum based on the Primakoff process is the same that was used in previous papers of this series [13]

$$\frac{d\Phi_a}{dE} = 6.02 \times 10^{10} g_{10}^2 \frac{E^{2.481}}{e^{E/1.205}} \text{ cm}^{-2}\,\text{s}^{-1}\,\text{keV}^{-1} \quad (5)$$

with $g_{10} = g_{a\gamma}/(10^{-10}\ \text{GeV}^{-1})$ and energies in keV. This result applies to axions with masses much smaller than the solar interior temperature, i.e., for sub-keV masses.

As explained in Ref. [14], the m_a dependence of the above expression is encoded in the probability $P_{a\to\gamma}$, which is coherently enhanced for values of m_a matching the refractive photon mass m_γ induced by the buffer gas density, while it is negligible for values away from m_γ. Therefore, only the counts observed with the gas density matching a given axion mass m_a will contribute to $\log \mathcal{L}$ (and the exclusion plot) for that mass m_a. We stress that the value of m_γ to be introduced is time dependent even within a single density step, due to the pressure excursions explained above.

Maximization of $\mathcal{L}$ (for a fixed value of m_a) leads to a best-fit value of g^4_{min}. The obtained value is compatible with the absence of a signal in the entire mass range, and, therefore, an upper limit on g^4 is obtained by integration of the Bayesian probability from zero up to 95% of its area in g^4. This is computed for many values of the axion mass m_a in order to configure the full exclusion plot shown in Fig. 1. A close up of the same exclusion plot is shown in Fig. 2,

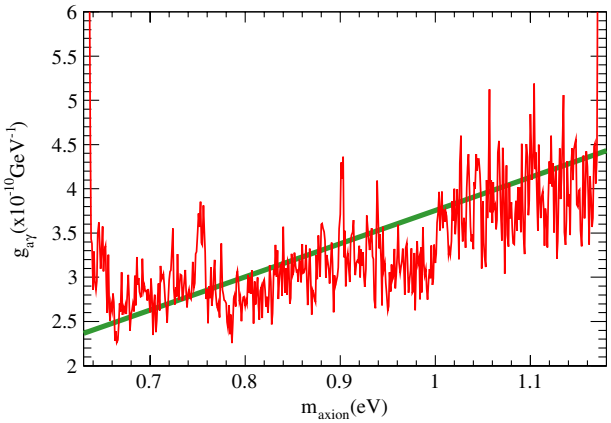

FIG. 2 (color online). Expanded view of the limit achieved in the CAST ^{3}He phase for the axion mass range between 0.64 and 1.17 eV, which corresponds to a pressure scan in ^{3}He from 36 to 105 mbar approximately. The actual limit contour has a high-frequency structure that is a result of statistical fluctuations that occur when a limit is computed for a specific mass using only a few hours of data. The green solid line corresponds to $E/N = 0$ (KSVZ model).

focused specifically in the axion mass range that has been explored in the data presented here.

As can be seen in Fig. 1, CAST extends its previous range towards higher axion masses, excluding the interval 0.64–1.17 eV down to an average value of the axion-photon coupling of 3.3×10^{-10} GeV^{-1}. The actual limit contour has a high-frequency structure that is a result of statistical fluctuations that occur when a limit is computed for a specific mass using only a few hours of data. The apparent slope upwards in the exclusion line for higher axion masses is due to the reduction of the exposure time per density step, for $m_a > 1$ eV, as well as to the continuous decrease of L_{eff} and the increase of Γ for higher gas densities. Eventually, with the addition of the data from the CCD/Telescope system, these numbers will likely improve.

Conclusions.—CAST has finished its phase of using ^{3}He buffer gas, continuing the search to its limiting pressure setting corresponding to a search mass of $m_a = 1.17$ eV. In this way, the search range now generously overlaps with the current cosmic hot dark matter bound of $m_a \lesssim 0.9$ eV and there would be little benefit in pushing to yet larger masses with the buffer-gas technique. CAST has not found axions and the next challenge is to move down in the m_a-$g_{a\gamma}$ plot to reach the "axion band" of theoretical models in a broader range of masses. Such a goal cannot be achieved with the existing CAST apparatus and will require significant improvements of detector and magnet properties, such as the proposed International AXion Observatory [44,45] or a completely new approach.

We thank CERN for hosting the experiment and for the technical support to operate the magnet and cryogenics. We thank the CERN CFD team for their essential contribution

to the CFD work. We acknowledge support from NSERC (Canada), MSES (Croatia) under the grant number 098-0982887-2872, CEA (France), BMBF (Germany) under the grant numbers 05 CC2EEA/9 and 05 CC1RD1/0 and DFG (Germany) under grant numbers HO 1400/7-1 and EXC-153, GSRT (Greece), NSRF: Heracleitus II, RFFR (Russia), the Spanish Ministry of Economy and Competitiveness (MINECO) under Grants No. FPA2008-03456 and No. FPA2011-24058. This work was partially funded by the European Regional Development Fund (ERDF/FEDER), the European Research Council (ERC) under grant ERC-2009-StG-240054 (T-REX), Turkish Atomic Energy Authority (TAEK), NSF (USA) under Award No. 0239812, U.S. Department of Energy, NASA under the grant number NAG5-10842. Part of this work was performed under the auspices of the U.S. Department of Energy by Lawrence Livermore National Laboratory under Contract No. DE-AC52-07NA27344. We acknowledge the helpful discussions within the network on direct dark matter detection of the ILIAS integrating activity (Contract No. RII3-CT-2003-506222).

[a]Present address: Bogazici University, Istanbul, Turkey.
[b]Present address: School of Physics and Astronomy, Schuster Laboratory, University of Manchester, Manchester, United Kingdom.
[c]Corresponding author. Theopisti.Dafni@unizar.es
[d]Present address: European Spallation Source ESS AB, Lund, Sweden.
[e]Present address: Laboratoire de l'Accélérateur Linéaire (LAL), Orsay, France.
[f]Also at Laboratoire de Transfert de Chaleur et de Masse, École Polytechnique Fédérale de Lausanne (EPFL), Lausanne, Switzerland.
[g]Present address: PNSensor GmbH, München, Germany.
[h]Present address: European XFEL GmbH, Notkestrasse 85, 22607 Hamburg, Germany.
[i]Present address: Physics Department and Center for Micro and Nano Sciences and Technologies, University of Rijeka, Radmile Matejcic 2, 51000 Rijeka, Croatia.
[j]Present address: Excellence Cluster Universe, Technische Universität München, Garching, Germany.
[k]Also at Physics Department, Ben-Gurion University of the Negev, Beer-Sheva 84105, Israel.
[l]Also at School of Space Research, Kyung Hee University, Yongin, Republic of Korea.
[m]Present address: University of California Berkeley, California 94720, California, USA.

[1] J. Jaeckel and A. Ringwald, Annu. Rev. Nucl. Part. Sci. **60**, 405 (2010).
[2] A. Ringwald, Phys. Dark Univ. **1**, 116 (2012).
[3] J. L. Hewett *et al.*, arXiv:1205.2671.
[4] P. Brun, J. Phys. Conf. Ser. **460**, 012015 (2013).
[5] P. Sikivie, Phys. Rev. Lett. **51**, 1415(E) (1983); **52**, 695 (1984).
[6] G. Raffelt and L. Stodolsky, Phys. Rev. D **37**, 1237 (1988).
[7] S. J. Asztalos, L. J. Rosenberg, K. van Bibber, P. Sikivie, and K. Zioutas, Annu. Rev. Nucl. Part. Sci. **56**, 293 (2006).
[8] D. M. Lazarus, G. Smith, R. Cameron, A. Melissinos, G. Ruoso, Y. Semertzidis, and F. Nezrick, Phys. Rev. Lett. **69**, 2333 (1992).
[9] S. Moriyama, M. Minowa, T. Namba, Y. Inoue, Y. Takasu, and A. Yamamoto, Phys. Lett. B **434**, 147 (1998).
[10] Y. Inoue, T. Namba, S. Moriyama, M. Minowa, Y. Takasu, T. Horiuchi, and A. Yamamoto, Phys. Lett. B **536**, 18 (2002).
[11] Y. Inoue, Y. Akimoto, R. Ohta, T. Mizumoto, A. Yamamoto, and M. Minowa, Phys. Lett. B **668**, 93 (2008).
[12] K. Zioutas *et al.* (CAST Collaboration), Phys. Rev. Lett. **94**, 121301 (2005).
[13] S. Andriamonje *et al.* (CAST Collaboration), J. Cosmol. Astropart. Phys. 04 (2007) 010.
[14] E. Arik *et al.* (CAST Collaboration), J. Cosmol. Astropart. Phys. 02 (2009) 008.
[15] M. Arik *et al.* (CAST Collaboration), Phys. Rev. Lett. **107**, 261302 (2011).
[16] K. Van Bibber, N. R. Dagdeviren, S. E. Koonin, A. K. Kerman, and H. N. Nelson, Phys. Rev. Lett. **59**, 759 (1987).
[17] J. Redondo and A. Ringwald, Contemp. Phys. **52**, 211 (2011).
[18] R. Bähre *et al.*, JINST **8**, T09001 (2013).
[19] A. Payez, J. R. Cudell, and D. Hutsemekers, J. Cosmol. Astropart. Phys. 07 (2012) 041.
[20] A. De Angelis, G. Galanti, and M. Roncadelli, Phys. Rev. D **84**, 105030 (2011).
[21] D. Horns, L. Maccione, M. Meyer, A. Mirizzi, D. Montanino, and M. Roncadelli, Phys. Rev. D **86**, 075024 (2012).
[22] M. Meyer, D. Horns, and M. Raue, Phys. Rev. D **87**, 035027 (2013).
[23] S. J. Asztalos *et al.* (ADMX Collaboration), Phys. Rev. Lett. **104**, 041301 (2010).
[24] J. Hoskins *et al.*, Phys. Rev. D **84**, 121302 (2011).
[25] S. J. Asztalos *et al.*, Nucl. Instrum. Methods Phys. Res., Sect. A **656**, 39 (2011).
[26] O. K. Baker, M. Betz, F. Caspers, J. Jaeckel, A. Lindner, A. Ringwald, Y. Semertzidis, P. Sikivie, and K. Zioutas, Phys. Rev. D **85**, 035018 (2012).
[27] D. Horns, J. Jaeckel, A. Lindner, A. Lobanov, J. Redondo, and A. Ringwald, J. Cosmol. Astropart. Phys. 04 (2013) 016.
[28] K. van Bibber, P. M. McIntyre, D. E. Morris, and G. G. Raffelt, Phys. Rev. D **39**, 2089 (1989).
[29] G. G. Raffelt, Lect. Notes Phys. **741**, 51 (2008).
[30] A. Friedland, M. Giannotti, and M. Wise, Phys. Rev. Lett. **110**, 061101 (2013).
[31] S. Hannestad, A. Mirizzi, G. G. Raffelt, and Y. Y. Y. Wong, J. Cosmol. Astropart. Phys. 08 (2010) 001.
[32] J. E. Kim, Phys. Rev. Lett. **43**, 103 (1979).
[33] M. A. Shifman, A. I. Vainshtein, and V. I. Zakharov, Nucl. Phys. **B166**, 493 (1980).
[34] S. Chang, Phys. Lett. B **316**, 51 (1993).
[35] S. Hannestad, A. Mirizzi, and G. Raffelt, J. Cosmol. Astropart. Phys. 07 (2005) 002.
[36] A. Melchiorri, O. Mena, and A. Slosar, Phys. Rev. D **76**, 041303 (2007).

[37] M. Archidiacono, S. Hannestad, A. Mirizzi, G. Raffelt, and Y. Y. Y. Wong, J. Cosmol. Astropart. Phys. 10 (2013) 020.
[38] M. Kuster *et al.*, New J. Phys. **9**, 169 (2007).
[39] P. Abbon *et al.*, New J. Phys. **9**, 170 (2007).
[40] S. Andriamonje *et al.*, JINST **5**, P02001 (2010).
[41] J. Galan *et al.*, JINST **5**, P01009 (2010).
[42] S. Aune *et al.* (CAST Collaboration), Nucl. Instrum. Methods Phys. Res., Sect. A **604**, 15 (2009).
[43] E. W. Lemmon (NIST) (private communication).
[44] I. G. Irastorza *et al.*, J. Cosmol. Astropart. Phys. 06 (2011) 013.
[45] I. Shilon, A. Dudarev, H. Silva, and H. H. J. ten Kate, IEEE Trans. Appl. Supercond. **23**, 4500604 (2013).